Deformation of C isotopes

Y. Kanada-En'yo
Institute of Particle and Nuclear Studies, High Energy Accelerator Research Organization, Ibaraki 305-0801, Japan
(Received 3 August 2004; published 24 January 2005)

Systematic analysis of the deformations of proton and neutron densities in even-even C isotopes was performed based on a method of antisymmetrized molecular dynamics. $E2$ transition strengths were discussed in relation to the deformations. We analyzed the $B(E2; 2_1^+ \to 0_1^+)$ in ^{16}C, which has been found to be abnormally small in the recent measurement. The results suggest a difference between proton and neutron shapes in the neutron-rich C isotopes. It was found that the stable proton structure in C isotopes plays an important role in the enhancement of the neutron skin structure as well as in the systematics of $B(E2)$ in the neutron-rich C.

DOI: 10.1103/PhysRevC.71.014310 PACS number(s): 21.60.−n, 02.70.Ns, 21.10.Ky, 27.20.+n

I. INTRODUCTION

In light unstable nuclei, exotic phenomena such as neutron halo and neutron skin structures were discovered owing to advancements in experimental technique. These phenomena contradict traditional understanding of stable nuclei, where the proton and neutron densities are consistent with each other in a nucleus. These phenomena imply that the exotic features may appear in unstable nuclei due to the difference between proton and neutron densities. The difference in the deformations of proton and neutron densities is also interesting. For example, opposite deformations in proton and neutron shapes in proton-rich C isotopes have been theoretically suggested [1].

Recently, the lifetime of the 2_1^+ state of ^{16}C has been measured [2]. It indicates the abnormally small $E2$ transition strength as $B(E2; 2_1^+ \to 0_1^+) = 0.63$ e^{2}fm^4 in ^{16}C, compared with those for other C isotopes (^{10}C, ^{12}C, and ^{14}C). As well known, $B(E2)$ is related to the intrinsic deformation of the nucleus. Considering the excitation energy $E_x(2_1^+) =$ 1.766 MeV of ^{16}C, it is expected that this nucleus is not spherical but has a deformed structure. In the case of normal stable nuclei, $B(E2)$ values tend to be large in the deformed nuclei. This means that the hindrance of the $B(E2; 2_1^+ \to 0_1^+)$ in ^{16}C seems to contradict the large deformation expected from the excitation energy ($E_x(2_1^+)$). The neutron and proton transition matrix elements M_n and M_p have been derived from the ^{208}Pb+^{16}C inelastic scattering [3], which implies that the neutron excitation is dominant in the 2_1^+ state of ^{16}C. In the context of collective rotation, these experimental results suggest a possible difference between proton and neutron shapes in ^{16}C. Similar behavior of the lowest 2^+ states, which have a low excitation energy and small $B(E2)$ values, is also seen in certain neutron-rich nuclei in the heavier mass number region. Such unusual properties of the first 2^+ states in ^{68}Ni and Te isotopes ($A \sim 132$) have been theoretically described by the neutron dominance in the 2^+ excitation [4,5].

In theoretical work on the proton-rich C isotopes [1], it was suggested that the different shapes of proton and neutron densities may cause the suppression of $B(E2)$. In this work [1], the difference between the proton and neutron shapes was also predicted for the neutron-rich C isotopes as well as for the proton-rich side. It is natural to consider that the systematic analysis of the proton and neutron deformations in connection to the $B(E2)$ is key to understanding the properties of the neutron-rich C isotopes. Moreover, it may lead to further predictions of exotic phenomena in unstable nuclei.

In this paper, we study deformations of proton and neutron densities in C isotopes based on theoretical calculations with antisymmetrized molecular dynamics (AMD). The AMD method is a useful approach for the structure study of stable and unstable nuclei. The applicability of this method in the systematic analysis of the light nuclei has been proven in many works [6–10]. In particular, this method has an advantage in the description of the deformation and clustering aspect in light nuclei. For example, an oblate deformation with a 3α-cluster structure in the ground state of ^{12}C has been described [7,11]. Although shell model calculations are useful for investigating the level structure of light nuclei, they are not suitable for direct discussion of the deformations of proton and neutron densities because electric moments are calculated with effective charges, which still have an ambiguity in the region of unstable nuclei in the framework. In order to extract a naive picture of the proton and neutron shapes, we apply the simplest version of AMD, based on a single AMD wave function. By using the AMD method, we analyze the systematics of the deformations and $E2$ transition strengths in neutron-rich C isotopes. The hindrance of the $E2$ transition strength in ^{16}C is discussed. The theoretical predictions for the deformation and $B(E2)$ values in additional neutron-rich isotopes, ^{18}C and ^{20}C, are also reported.

This paper is organized as follows. In Sec. II, the formulation of AMD is briefly explained. We show the energies, radii, and $B(E2)$ values obtained by the simple version of AMD and compare them with the experimental data in Sec. IV. In Sec. V, the intrinsic deformations of proton and neutron densities are analyzed in connection to observables such as the $E2$ and radii. In Sec. VI, we show the results of ^{16}C obtained by an extended version of AMD. Finally, a summary is given in Sec. VII.

II. FORMULATION

The detailed formulation of AMD for nuclear structure studies is described in [6,8,11]. Here, we briefly explain the formulation of the present calculations.

The wave function of a system with mass number A is written by a superposition of AMD wave functions $\Phi_{\rm AMD}$. An AMD wave function is given by a single Slater determinant of Gaussian wave packets as

$$\Phi_{\rm AMD}(\mathbf{Z}) = \frac{1}{\sqrt{A!}}\mathcal{A}\{\varphi_1, \varphi_2, \ldots, \varphi_A\}, \tag{1}$$

where the i-th single-particle wave function is written as

$$\varphi_i = \phi_{\mathbf{X}_i}\chi_i\tau_i, \tag{2}$$

$$\phi_{\mathbf{X}_i}(\mathbf{r}_j) \propto \exp\left\{-\nu\left(\mathbf{r}_j - \frac{\mathbf{X}_i}{\sqrt{\nu}}\right)^2\right\}, \tag{3}$$

$$\chi_i = \left(\frac{1}{2} + \xi_i\right)\chi_\uparrow + \left(\frac{1}{2} - \xi_i\right)\chi_\downarrow. \tag{4}$$

In the AMD wave function, the spatial part is represented by complex variational parameters, X_{1i}, X_{2i}, X_{3i}, which indicate the center of the Gaussian wave packet. The orientation of the intrinsic spin is expressed by a variational complex parameter ξ_i, and the isospin function is fixed to be up(proton) or down(neutron). Thus, an AMD wave function is expressed by a set of variation parameters: $\mathbf{Z} \equiv \{\mathbf{X}_1, \mathbf{X}_2, \cdots, \mathbf{X}_A, \xi_1, \xi_2, \cdots, \xi_A\}$.

In order to obtain a naive understanding of the systematics of intrinsic deformations, we use the simplest version of the AMD method, which was applied to Li, Be, and B isotopes in Ref. [6]. Namely, we perform energy variation with respect to a parity-eigen state, $P^\pm\Phi_{\rm AMD} \equiv \Phi^\pm_{\rm AMD}$, projected from an AMD wave function. We consider the AMD wave function obtained by the energy variation as the intrinsic state, and the total-angular-momentum projection (P^J_{MK}) is done after the variation to evaluate observables such as the energies, radii, and transition strength. Thus the variation is done after the parity projection, but the total-angular-momentum projection is performed after the variation. This method is called VBP (variation before projection) in the present paper. For further investigation of the level scheme of ^{16}C, we also perform the VAP (variation after full projection) calculation with respect to both the parity and total-angular-momentum projection in the same way as done in Refs. [11,12]. In the VBP calculations, we fix the orientation of the intrinsic spin ξ_i to be up or down. In the VAP calculations, ξ_i's are treated as free variational parameters.

III. INTERACTIONS

The effective nuclear interactions adopted in the present work consist of the central force, the spin-orbit force, and the Coulomb force. We adopt the MV1 force [13] as the central force. This central force contains a zero-range three-body force as a density-dependent term in addition to the two-body interaction. The Bartlett and Heisenberg terms are chosen to be $b = h = 0$. We use the parameter set of case 3 of the MV1 force with the Majorana parameter as $m = 0.576$, which was adopted in Ref. [6]. Concerning the spin-orbit force, the same form of the two-range Gaussian as of the G3RS force [14] is adopted. The strengths of the spin-orbit force—(a) $u_{1s} \equiv u_I = -u_{II} = 900$, and (b) 1500 MeV—are used. In the VAP calculations, we also use the same interaction parameters as those used in Ref. [11]: (c) case 1 of the MV1 force with $m = 0.62$, and the spin-orbit force with $u_{ls} =$ 3000 MeV.

TABLE I. The adopted width parameters (ν) of the AMD wave functions for C isotopes.

	^{10}C	^{12}C	^{14}C	^{16}C	^{18}C	^{20}C
ν (fm^{-2})	0.185	0.190	0.180	0.175	0.170	0.165

IV. RESULTS OF VBP CALCULATIONS

The structure of positive parity states of even-even C isotopes are studied using VBP calculations within the framework of AMD. In this section, we present theoretical results, such as the energies, radii, and $E2$ transitions, and compare them with the experimental data. The optimum width parameter ν in Eq. (3) is chosen to minimize the energy of the system for each nucleus. The adopted ν parameters are listed in Table I. After the variation, we perform the total-angular-momentum projection P^J_{MK} and diagonalize the Hamiltonian and norm matrices, $\langle P^J_{MK'}\Phi^\pm_{\rm AMD}|H|P^J_{MK''}\Phi^\pm_{\rm AMD}\rangle$ and $\langle P^J_{MK'}\Phi^\pm_{\rm AMD}|P^J_{MK''}\Phi^\pm_{\rm AMD}\rangle$, with respect to the K-quantum (K', K''). In each C isotope, we obtain the 0^+_1 and 2^+_1 states, which can be regarded as belonging to the ground $K^\pi = 0^+$ band. In the cases of ^{10}C, ^{16}C, and ^{18}C, the second 2^+ state in the $K^\pi = 2^+$ band arises because of the axial asymmetry.

The binding energies and the excitation energies of the low-lying positive-parity states are shown in Fig. 1 and Table II, respectively. The binding energies of C isotopes are reasonably reproduced by the present calculations (Fig. 1). The agreement of the binding energy will be improved by finely tuning the interaction parameters such as Bartlett and Heisenberg terms, though it should make no drastic change of properties other than the binding energies. As mentioned above, the second 2^+ state, which belongs to the sideband $K^\pi = 2^+$, is found in addition to the 2^+_1 state, in ^{10}C, ^{16}C, and ^{18}C (Table II).

The excitation energies E_x of the 2^+_1 states tend to be underestimated by the calculations, especially in the

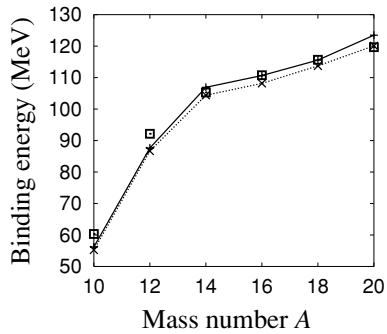

FIG. 1. Binding energies of C isotopes. Solid (dotted) line indicates the VBP calculations with $m = 0.576$ and $u_{ls} =$ 1500 (900) MeV. The squares denote the experimental data.

TABLE II. Excitation energies of 2^+ states of C isotopes obtained by the VBP calculations.

		^{10}C	^{12}C	^{14}C	^{16}C	^{18}C	^{20}C
Cal. ($ls = 900$ MeV)	$E_x(2_1^+)$ (MeV)	1.80	1.45	1.69	0.40	0.61	0.57
	$E_x(2_2^+)$ (MeV)	2.60	—	—	1.53	0.83	—
Cal. ($ls = 1500$ MeV)	$E_x(2_1^+)$ (MeV)	1.95	1.66	3.75	0.65	0.87	0.88
	$E_x(2_2^+)$ (MeV)	3.75	—	—	2.82	1.32	—
Exp.	$E_x(2_1^+)$ (MeV)	3.354	4.439	7.012	1.766	1.59[a]	1.59[a]
	$E_x(2_2^+)$ (MeV)	6.58	—	—	—	—	—

[a]The data are from Ref. [15].

neutron-rich C isotopes. This is a general tendency of the VBP calculations where the 0_1^+ and 2_1^+ states are obtained by the total-angular-momentum projection from a single intrinsic wave function. This tendency is considered to be because the wave function obtained in the VBP may be optimized for the 2_1^+ state rather than for the 0_1^+ state; therefore, the energy of the 0_1^+ state may be relatively higher. The quantitative reproduction of $E_x(2_1^+)$ is improved by VAP calculations. The level structure of ^{16}C is discussed again in Sec. VI based on the VBP and VAP calculations.

Figure 2 shows the results for the root-mean-square radii compared with the experimental ones derived from the interaction cross sections. In the systematics of the matter radii in the even-even C isotopes, there is a gap between ^{14}C and ^{16}C. This behavior is reproduced by the present calculations and can be described by the large deformation in ^{16}C and the spherical shape due to the shell closure in ^{14}C. The details are discussed in the next section.

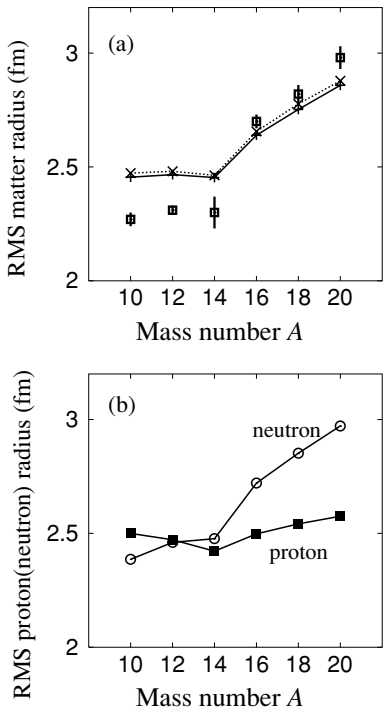

FIG. 2. Root-mean-square radii of C isotopes. The matter radii are displayed in the upper panel (a). The solid (dotted) line with symbols "+(×)' indicates the VBP calculations with $m = 0.576$ and $u_{ls} = 1500(900)$ MeV. The experimental data, which are derived from the interaction cross sections [16], are shown by open squares. The point-like proton and neutron radii calculated with $m = 0.576$ and $u_{ls} = 1500$ MeV are shown in the lower panel (b).

The results for the $E2$ transition strength are listed in Table III. In the calculations, it is found that $B(E2; 2_1^+ \to 0_1^+)$ drastically changes with the increase of neutron number in C isotopes. The theoretical $E2$ transition strength in ^{16}C is very small, which is consistent with the recent measurement of the abnormally small $B(E2)$ in ^{16}C [2]. The present results predict that $B(E2; 2_1^+ \to 0_1^+)$ in ^{18}C is also very small and of the same order as that in ^{16}C. It is interesting that the calculated $E2$ transition strength in ^{20}C is not as small as those in ^{16}C and ^{18}C. The systematic change of the $B(E2; 2_1^+ \to 0_1^+)$ can be understood by the deformations of proton and neutron densities in the intrinsic states, as described in the next section.

V. DISCUSSION

In this section, we analyze the intrinsic deformations of proton and neutron densities and discuss their effects on the observables such as the $E2$ transitions and radii.

A. Intrinsic deformation

In Fig. 3, we display the deformation parameters (β, γ) for the proton and neutron densities, which are defined by the moments $\langle x^2 \rangle$, $\langle y^2 \rangle$, and $\langle z^2 \rangle$ of the intrinsic AMD wave function as

$$\frac{\langle x^2 \rangle^{1/2}}{(\langle x^2 \rangle \langle y^2 \rangle \langle z^2 \rangle)^{1/6}} \equiv \exp\left[\sqrt{\frac{5}{4\pi}}\beta \cos\left(\gamma + \frac{2\pi}{3}\right)\right], \quad (5)$$

$$\frac{\langle y^2 \rangle^{1/2}}{(\langle x^2 \rangle \langle y^2 \rangle \langle z^2 \rangle)^{1/6}} \equiv \exp\left[\sqrt{\frac{5}{4\pi}}\beta \cos\left(\gamma - \frac{2\pi}{3}\right)\right], \quad (6)$$

$$\frac{\langle z^2 \rangle^{1/2}}{(\langle x^2 \rangle \langle y^2 \rangle \langle z^2 \rangle)^{1/6}} \equiv \exp\left[\sqrt{\frac{5}{4\pi}}\beta \cos\gamma\right]. \quad (7)$$

Here, the x, y, and z directions are chosen so as to satisfy $\langle x^2 \rangle \leqslant \langle y^2 \rangle \leqslant \langle z^2 \rangle$ and $\langle xy \rangle = \langle yz \rangle = \langle zx \rangle = 0$. As can be seen in Fig. 3, we find a drastic change of neutron deformation in C isotopes with an increase in the neutron number. The neutron deformations are prolate, oblate, and spherical in ^{10}C, ^{12}C, and ^{14}C, respectively. In the neutron-rich region, it

TABLE III. $E2$ transition strengths (e^2fm^4) in C isotopes calculated by the VBP. The experimental data for ^{16}C are from Ref. [2] and those for the other C isotopes are from Ref. [17].

		^{10}C	^{12}C	^{14}C	^{16}C	^{18}C	^{20}C
Cal. ($ls = 900$ MeV)	$B(E2; 2_1^+ \to 0_1^+)$	5.7	7.2	6.9	1.9	2.1	5.3
	$B(E2; 2_2^+ \to 0_1^+)$	4.3	—	—	4.7	3.8	—
Cal. ($ls = 1500$ MeV)	$B(E2; 2_1^+ \to 0_1^+)$	5.4	6.8	5.9	1.4	0.6	5.0
	$B(E2; 2_2^+ \to 0_1^+)$	3.4	—	—	4.1	4.9	—
Exp.	$B(E2; 2_1^+ \to 0_1^+)$	12.4 ± 0.2	8.2 ± 0.1	3.74 ± 0.5	0.63	—	—

becomes prolate again in ^{16}C, and they are triaxial and oblate in ^{18}C and ^{20}C, respectively. In contrast to the variation of the neutron deformations, the proton deformations are rather stable. The deformation parameters for the proton densities lie in the oblate region $\gamma \sim \pi/3$. This behavior is the same as the results found in Ref. [1].

By analyzing the component of the K-projected states ($P^J_{MK}\Phi^{\pm}_{\rm AMD}$) in the 2_1^+, it is found that the 2_1^+ state can be approximately written by a single $K = 0$ state when we choose a proper axis. Then, we can define the (approximate) principal axis Z in the body-fixed frame and form the ground $K = 0$ band with the 0_1^+ and 2_1^+ states in each C isotope. In the systems ^{12}C, ^{14}C, and ^{20}C, with the oblate or spherical neutron shapes, the principal axis Z is the same as the symmetric axis x which has the smallest moment $\langle x^2 \rangle$ as shown in Fig. 4(b). In other words, the dominant component of the excited state 2_1^+ is the $J_{Z=x} = K = 0$ state with respect to the symmetric axis x. It is consistent with a naive expectation for the collective rotation. It is notable that, in ^{10}C, ^{16}C, and ^{18}C, the deformations are different between proton and neutron densities. In these nuclei, the symmetric axis for the proton shape differs from that for neutron density. Namely, the symmetric axis of the oblate proton density orients toward the x direction, while that of the prolate neutron is in the z direction. A schematic figure for the proton and neutron shapes in ^{16}C is illustrated in Fig. 4(a). Such a configuration of the proton and neutron shapes is energetically favored because it has the maximum overlap between the proton and neutron densities. Because of the coexistence of the different proton and neutron shapes, the second 2^+ state appears, due to the triaxiality of the total system. With the analysis of the component of the $P^J_{MK}\Phi^{\pm}_{\rm AMD}$ states in the 2_1^+ and 2_2^+ states, we found that the 0_1^+ and 2_1^+ states form the $K^\pi = 0_1^+$ band while the 2_2^+ state is classified as the band-head state of the sideband $K^\pi = 2^+$ when we regard the longitudinal z axis as the principal axis Z as shown in Fig. 4(a). It is important that the principal axis Z is not the same as the symmetric axis x for the proton deformation but

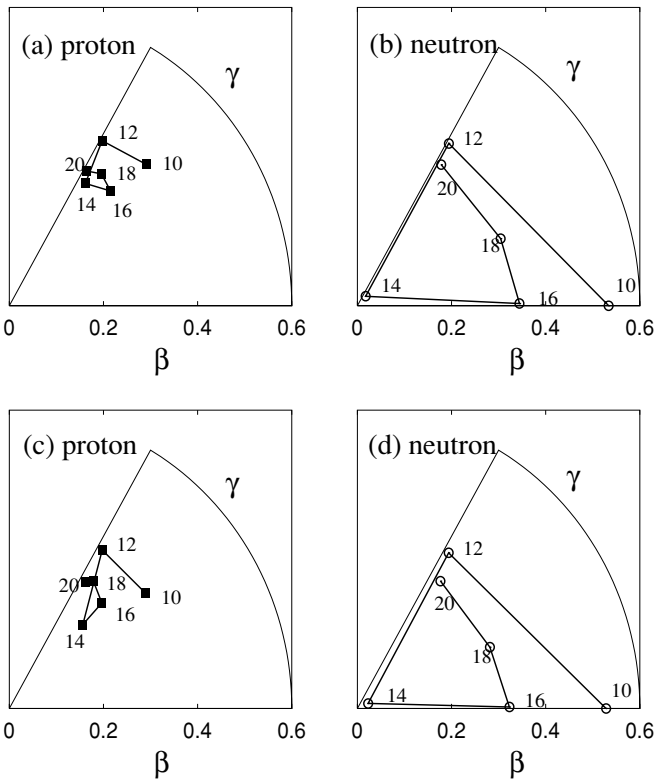

FIG. 3. Deformation parameters β, γ of the intrinsic states calculated with $m = 0.576$ and $u_{ls} = 900$ MeV (a, b) and 1500 MeV (c, d). The mass numbers A are written by the corresponding points. The left and right panels are (β, γ) for proton and neutron densities, respectively.

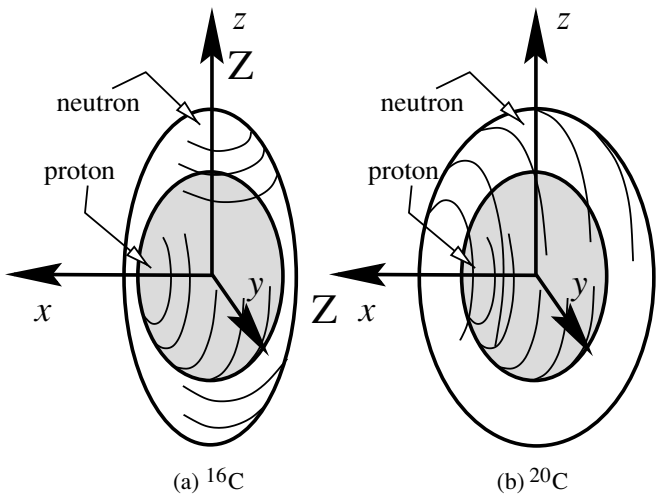

FIG. 4. Schematic figures for intrinsic deformations of the proton and neutron densities. (a) The oblate proton and prolate neutron shapes in ^{16}C, and (b) the oblate proton and oblate neutron densities in ^{20}C. The x, y, and z axes are chosen to be $\langle x^2 \rangle \leqslant \langle y^2 \rangle \leq \langle z^2 \rangle$. The principal axis Z for the ground band $J_Z = K^\pi = 0$ is also displayed.

is perpendicular to the x axis in these nuclei. The existence of the sideband ($K^\pi = 2^+$) in ^{16}C and ^{18}C has not been experimentally confirmed yet. Concerning ^{10}C, the triaxiality of the mirror nucleus ^{10}Be is discussed in Ref. [18], and the known 2_2^+ state in ^{10}Be is actually assigned to be the band-head state of the sideband $K^\pi = 2^+$ [12,18].

We compare the matter deformation of the present results with a HF+BCS calculation with Skyrme force by Tajima *et al*. [19]. In the HF+BCS calculation, the C isotopes have spherical shapes in the $A \leqslant 14$ region, in contradiction to the usual finding that ^{12}C is oblately deformed. It is natural because the mean-field calculation is not necessarily valid for very light nuclei. In the neutron-rich C, the calculated quadrupole deformation parameter is positive in ^{16}C and ^{18}C, and negative in ^{20}C according to the HF+BCS calculation. The general behavior of the quadrupole deformation for the matter density in neutron-rich C seems to be similar to that in the present results, though the difference in shape between proton and neutron hardly appears in the HF calculations.

B. $E2$ transition

The intrinsic deformation is closely related to the $E2$ transition strength. Since the present results indicate that the proton radius does not drastically change with the increase of the neutron number in C isotopes as shown in Fig. 2, the $B(E2)$ is dominantly determined by the deformations.

As mentioned above, the 0_1^+ and 2_1^+ states belong to the ground $K^\pi = 0^+$ band, where the x axis is regarded as the principal axis Z in ^{12}C, ^{14}C, and ^{20}C, while the z axis corresponds to the Z axis in ^{10}C, ^{16}C, and ^{18}C. In order to link the intrinsic deformations with the $B(E2)$ values, we remind the reader of the well known approximate relation between the $B(E2)$ values and the intrinsic quadrupole moment Q_0:

$$B\left(E2; 2_1^+ \to 0_1^+\right) = \frac{1}{16\pi} e^2 Q_0^2. \tag{8}$$

Here, the intrinsic quadrupole moment Q_0 of protons is defined with respect to the principal axis Z as $Q_0 = 2\langle Z^2\rangle - \langle X^2\rangle - \langle Y^2\rangle$ and is related to the deformation parameter β_p, γ_p for the proton shape. In ^{12}C, ^{14}C, and ^{20}C with $Z \approx x$ and $\gamma \approx \pi/3$, Q_0 is approximated as

$$Q_0 = 2\langle x^2\rangle - \langle y^2\rangle - \langle z^2\rangle \approx -\sqrt{\frac{5}{4\pi}} N_p e \beta_p r_e^2, \tag{9}$$

where N_p and r_e are the proton number and the root-mean-square charge radius, respectively.

In ^{10}C, ^{16}C, and ^{18}C with $Z \approx z$, Q_0 depends on the deformation parameter γ_p, as

$$Q_0 = 2\langle z^2\rangle - \langle x^2\rangle - \langle y^2\rangle \approx \sqrt{\frac{5}{4\pi}} N_p e \beta_p \cos\gamma_p r_e^2. \tag{10}$$

The important point is that the effect of the proton deformation on the Q_0 decreases in these nuclei because of the factor $\cos\gamma_p$. Especially in ^{16}C and ^{18}C, the deformation parameter $\gamma_p \sim \pi/3$ makes the Q_0 very small. This is the reason for the unusually small $B(E2; 2_1^+ \to 0_1^+)$ in ^{16}C and ^{18}C shown in Table III. In other words, the $B(E2; 2_1^+ \to 0_1^+)$ values in ^{16}C and ^{18}C are reduced because the principal axis Z for the rotation of the total system deviates from the symmetric axis x for the proton density. The origin of the deviation is the difference in shape between proton and neutron densities. On the other hand, it is interesting that the larger $B(E2 : 2_1^+ \to 0_1^+)$ is predicted in ^{20}C because it has the oblate proton and neutron shapes, and therefore the principal axis aligns to the symmetric axis x as shown in Fig. 4(b).

The hindrance of the $B(E2 : 2_1^+ \to 0_1^+)$ in ^{16}C can also be described from the point of view of the collective rotation. The 2_1^+ state of ^{16}C is roughly regarded as the 2^+ state with $J_z = K = 0$. The $J = 2, J_z = 0$ state is given by a linear combination of a $J_x = 2$ state and a $J_y = 2$ state, which are rotating around the x and y axes, respectively. The rotational motion around the x axis causes no proton excitation and therefore does not contribute to the $E2$ transition strength, because x is the symmetric axis of proton density. As a result, the $J_x = 2$ component reduces the $B(E2 : 2_1^+ \to 0_1^+)$ value. In contrast to the small $B(E2 : 2_1^+ \to 0_1^+)$, the $B(E2 : 2_2^+ \to 0_1^+)$ in the sideband is predicted to be large because the 2_2^+ state is dominated by a $J_z = 2$ state, which contains the proton excitations rather than the neutron excitations.

As mentioned above, the abnormally small $B(E2 : 2_1^+ \to 0_1^+)$ in ^{16}C can be understood by the difference between oblate proton and prolate neutron shapes. Even if the proton shape in ^{16}C is spherical or slightly prolate, the small $B(E2 : 2_1^+ \to 0_1^+)$ can also be described. Therefore, we cannot conclude that the small $B(E2)$ is evidence of an oblate proton shape. However, we would like to stress that a characteristic of the present result is the stable proton structure in the series of C isotopes, which leads to the appearance of the second 2^+ state with large $B(E2)$ appears in the sideband. In order to determine the intrinsic shapes of proton and neutron densities, we need further experimental information such as the systematics of $B(E2)$ in other neutron-rich nuclei and some probes for the sideband in ^{16}C.

C. Radii

In Fig. 2, we present the calculated results of matter, proton, and neutron radii of C isotopes while comparing them with the experimental radii which are derived from the interaction cross sections [16]. With the increase of neutron number, the proton radius does not drastically change, while the neutron radius increases rapidly in the neutron-rich $A \geqslant 16$ region. It is found that the gap of the matter radii between ^{14}C and ^{16}C originates in the neutron radii. The reason for the gap is described by the change of the neutron shape as follows. The neutron density is compact in ^{14}C because it has a spherical shape due to the neutron shell closure. On the other hand, in ^{16}C, the neutron radii is large because of the prolate deformation.

The calculated matter radii systematically reproduce the experimental data. The large matter radii in the neutron-rich region originate from the enhancement of the neutron radii. In contrast to the variation of the neutron radii, the proton radius is stable and is compact in general. As a result of the stable proton structure, the neutron skin structure is enhanced in the neutron-rich C isotopes. The present finding of the development of

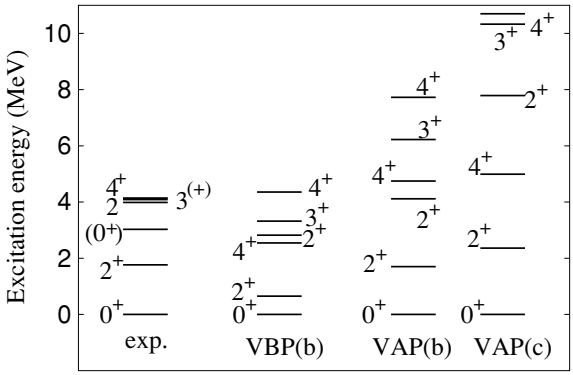

FIG. 5. Level scheme of the low-lying states of ^{16}C. The theoretical results obtained by the VAP and VBP calculations with the interaction parameter set (b) as in case 3 of MV1 with $m = 0.576$, $u_{ls} = 1500$ MeV and parameter set (c) as in case 1 of MV1 with $m = 0.62, u_{ls} = 3000$ MeV are illustrated with the experimental data.

neutron skin in the C isotopes is consistent with those of the mean-field calculations [19]. In the calculations by Thiamova *et al*. [10] with AMD+GCM (generator coordinate method), the radii of neutron-rich C are somehow underestimated. This is considered to be because of the lack of the three-body term in the effective force in their calculations.

VI. RESULTS OF VAP CALCULATION

So far, we discuss the structure of C isotopes based on the VBP calculations. As mentioned above, the quantitative reproduction of the excitation energy $E_x(2_1^+)$ in the VBP calculations is not satisfactory in the neutron-rich C. Instead, the VAP calculation [11,12] is more useful to describe the detail of the level spacing. We perform energy variation after the spin-parity projection for the 0_1^+, 2_1^+, and 2_2^+ states of ^{16}C and obtain three independent AMD wave functions, each of which is optimized for the corresponding spin-parity states. We evaluate the observables by diagonalizing the Hamiltonian and norm matrices with respect to the three wave functions, as done in Refs. [11,12].

Figure 5 shows the level scheme of the low-lying states of ^{16}C obtained by the VBP and VAP calculations with interaction parameter set (b) as in MV1 (case 3) with $m = 0.576$, $u_{ls} =$ 1500 MeV. We also show the VAP results obtained by the other parameter set (c) as in MV1 (case 1) with $m = 0.62$, $u_{ls} = 3000$ MeV, which were adopted in Ref. [11] to reproduce well the level structure of ^{12}C. The level spacing between the 0_1^+ and 2_1^+ states is well reproduced by the VAP calculations. The excitation energies of the sideband $K^\pi = 2^+$ states rise compared to those with VBP. Specifically, in the VAP with the interaction parameter set (c), the 2_2^+ state becomes relatively high because of the strong spin-orbit force.

The results of the $E2$ transition strength in ^{16}C are listed in Table IV. Comparing the theoretical values with the experimental data, the VAP calculations tend to overestimate $B(E2; 2_1^+ \to 0_1^+)$. In the results of ^{16}C, it should be noted that the beta deformation β_p for the proton density in the VAP(b) is almost the same as that in the VBP(b); however, the

TABLE IV. The $E2$ transition strength in ^{16}C. The theoretical results are obtained by the VAP and VBP calculations with the interaction parameter set (b) of $m = 0.576$, $u_{ls} = 1500$ MeV and set (c) of $m = 0.62$, $u_{ls} = 3000$ MeV. The unit is $e^2\text{fm}^4$.

	Exp.	VBP(b)	VAP(b)	VAP(c)
$B(E2; 2_1^+ \to 0_1^+)$	0.63	1.4	3.7	2.7
$B(E2; 2_r^+ \to 0_1^+)$	—	4.1	2.0	2.6

γ deformation γ_p in the VAP(b) differs from that in the VBP(b). Namely, the triaxial shape $\gamma_p \sim \pi/6$ of the proton density is found in the VAP results, whereas it is oblate, as $\gamma_p \sim \pi/3$, in the VBP results. This is the reason for the larger $B(E2; 2_1^+ \to 0_1^+)$ in VAP than in VBP because the factor $\beta_p \cos\gamma_p$ in Eq. (10) increases due to the triaxial deformation. Instead, the $E2$ transition in the sideband, $B(E2; 2_2^+ \to 0_1^+)$, is smaller in the VAP than in the VBP because of the triaxiality of the proton shape.

As already mentioned in Sec. IV, the VBP calculations underestimate the excitation energy $E_x(2_1^+)$, whereas the reproduction of $E_x(2_1^+)$ is improved in the VAP calculations. In the 2_1^+ state of ^{16}C, the neutron excitation is found to be dominant in both the VBP and VAP calculations. Since the deformation parameter β_n for the neutron density in the VAP(b) is consistent with that in the VBP(b), the discrepancy of the $E_x(2_1^+)$ between the VBP and VAP cannot be simply explained in terms of the intrinsic deformations. The reason for the underestimation of $E_x(2_1^+)$ in the VBP is considered to be that the wave function may be better optimized for the 2_1^+ state than for the 0_1^+ state within the VBP framework, where the spin-eigen states are obtained by the total-angular-momentum projection from a single intrinsic wave function after the variation. By comparing the energies of the 0_1^+ and 2_1^+ states between VAP and VBP, it is found that the energy gain from VBP to VAP is larger in the 0_1^+ state than in the 2_1^+ state as the gains are 5.4 and 3.3 MeV for the 0_1^+ and 2_1^+ states, respectively. Since the VBP calculations relatively overestimate the energy of the 0_1^+ state, they give a small level spacing between the 2_1^+ and 0_1^+ states. The experimental $E_x(2_1^+)$ is well reproduced by VAP calculations, where the wave function is optimized for each spin-parity state. We would like to comment that, although the level spacing of the VBP in ^{16}C does not quantitatively agree with that of the VAP, the wave functions for the 0_1^+, 2_1^+, and 4_1^+ obtained by the VAP(b) still have large overlap with the VBP(b) wave functions as 72%, 77%, and 86%, respectively.

In the present VAP calculations of ^{16}C, the 0_1^+ and 2_1^+ level spacing is well reproduced, while the reproduction of the small $B(E2; 2_1^+ \to 0_1^+)$ is not satisfactory. We note that the AMD+GCM calculations with the Volkov force reproduce the $E_x(2_1^+)$ of C isotopes [10], although the radii of the neutron-rich C are underestimated with this interaction. When we use the present interaction parameter set (b) where $m = 0.576$ and $u_{ls} = 1500(900)$ MeV, the results of $E_x(2_1^+)$ and $B(E2)$ for ^{16}C obtained by a AMD+GCM method [20] are similar to those of the VBP calculations. In order to gain insight into the structure of ^{16}C, we need to improve wave functions by producing them in more detail. Moreover, further experimental information for

other excited states will be helpful in determining the proton shape in ^{16}C.

VII. SUMMARY

We studied the structure of even-even C isotopes with the AMD method. The systematics of the binding energies, $B(E2)$, and radii of C isotopes are qualitatively reproduced by the simplest version of AMD calculations (VBP). Systematic analysis of the proton and neutron shapes in C isotopes was done based on the VBP calculations of AMD. The results indicate that the neutron shape drastically changes with an increase of neutron number, while the proton shape is rather stable. It is suggested that the difference between proton and neutron shapes may appear in ^{16}C and ^{18}C as well as in ^{10}C. The $E2$ transition strength, $B(E2)$, was discussed in relation to the deformation. The unusually small $B(E2; 2^+_1 \to 0^+_1)$ in ^{16}C, which has been recently measured, was described by the coexistence of the oblate proton shape and the prolate neutron shape. According to the present prediction, the $B(E2; 2^+_1 \to 0^+_1)$ in ^{18}C is as small as that in ^{16}C, while the $B(E2)$ is larger in ^{20}C. The deviation between the proton and neutron shapes plays an important role in the small $B(E2)$. The present results show the enhancement of the neutron skin structure in neutron-rich C. It was found that the stable proton structure in C isotopes plays an important role in the neutron skin structure as well as in the systematics of $B(E2)$.

In order to extract a naive picture of the proton and neutron shapes, we applied the VBP method based on a single AMD wave function. The quantitative reproduction of the excitation energy ($E_x(2^+_1)$) was not satisfactory in the VBP calculations. We showed that the level structure of ^{16}C is well reproduced by VAP calculations, although they overestimate the $B(E2)$ of ^{16}C. We consider that, for further detailed investigations and better reproductions, it is important to improve the wave functions by superposing the basis and using appropriate effective nuclear forces.

Here, we would like to comment on *ab initio* calculations based on realistic nucleon-nucleon interactions, which have recently made remarkable progress. For example, the exact calculations of the ground state of ^{12}C have been performed with the Green's function Monte Carlo method [21]. Another *ab initio* approach for this mass number region is the large-basis no-core shell, which has been applied to ^{12}C [22]. In the study of cluster structure, Fermionic Molecular Dynamics (FMD) is a useful method where the effective force derived from realistic interactions is adopted [23]. In the results of ^{12}C obtained by FMD, various kinds of 3α-cluster structure were found in excited states, which are clearly consistent with those of AMD [11]. The application of these methods to neutron-rich C isotopes is requested.

In the experiment on ^{208}Pb+^{16}C inelastic scattering, the contributions of nuclear excitation and Coulomb excitation from the ground state to the 2^+_1 (1.77 MeV) state were analyzed [3]. The ratio of the neutron and proton transition matrix elements M_n/M_p implies the neutron excitation is dominant in the 2^+_1 state in ^{16}C. This is consistent with the present results of oblate proton and prolate neutron shapes. Unfortunately, with this experimental information for the excitation to the 2^+_1(1.77 MeV), it is difficult to know whether the proton deformation is oblate or slightly prolate (or slightly triaxial), because in both cases the sign of the $M_p(0^+_1 \to 2^+_1)$ is the same. Namely, even if the proton density has an oblate shape, the M_p is not a negative but a positive value because of the different orientations of the symmetric axes between the proton and neutron shapes as shown in Q_0 given by Eq. (10). A characteristic of the present result is the stable proton structure and systematics of $B(E2)$ in the series of C isotopes. If the ^{16}C has the oblate proton shape, the second 2^+ state appears. Whether the proton density is oblate or slightly prolate in ^{16}C, the small $B(E2)$ implies that the proton deformation must be inconsistent with the large prolate deformation of the neutron shape. Therefore, we conclude that the small $B(E2)$ indicates a difference between proton and neutron shapes in ^{16}C. In order to understand the details of the intrinsic shapes of proton and neutron densities, we need more systematic analysis of C isotopes with the help of further experimental information such as the $B(E2)$ in other neutron-rich nuclei, ^{18}C and ^{20}C, and information for the sideband in ^{16}C.

ACKNOWLEDGMENTS

The author would like to thank Prof. H. Horiuchi, Dr. M. Takashina, and Dr. N. Itagaki for many discussions. She is also thankful to Prof. T. Motobayashi, Dr. N. Imai, and Z. Elekes for valuable comments. The computational calculations in this work were supported by the Supercomputer Project Nos. 58, 70, 83, and 93 of the High Energy Accelerator Research Organization (KEK). This work was supported by the Japan Society for the Promotion of Science and a Grant-in-Aid for Scientific Research of the Japan Ministry of Education, Science and Culture. The work was partially performed in the "Research Project for Study of Unstable Nuclei from Nuclear Cluster Aspects" sponsored by the Institute of Physical and Chemical Research (RIKEN).

[1] Y. Kanada-En'yo and H. Horiuchi, Phys. Rev. C **55**, 2860 (1997).
[2] N. Imai *et al*., Phys. Rev. Lett. **92**, 062501 (2004).
[3] Z. Elekes *et al*., Phys. Lett. **B586**, 34 (2004).
[4] K. Langanke, J. Terasaki, F. Nowacki, D. J. Dean, and W. Nazarewicz, Phys. Rev. C **67**, 044314 (2003).
[5] J. Terasaki, J. Engel, W. Nazarewicz, and M. Stoitsov, Phys. Rev. C **66**, 054313 (2002).
[6] Y. Kanada-En'yo, H. Horiuchi, and A. Ono, Phys. Rev. C **52**, 628 (1995); Y. Kanada-En'yo and H. Horiuchi, Phys. Rev. C **52**, 647 (1995).
[7] Y. Kanada-En'yo and H. Horiuchi, Prog. Theor. Phys. Suppl. **142**, 205 (2001).
[8] Y. Kanada-En'yo, M. Kimura, and H. Horiuchi, C. R. Phys. **4**, 497 (2003).
[9] N. Itagaki and S. Aoyama, Phys. Rev. C **61**, 024303 (2000).

[10] G. Thiamova, N. Itagaki, T. Otsuka, and K. Ikeda, Nucl. Phys. **A719**, 312c (2003).
[11] Y. Kanada-En'yo, Phys. Rev. Lett. **81**, 5291 (1998).
[12] Y. Kanada-En'yo, H. Horiuchi, and A. Doté, Phys. Rev. C **60**, 064304 (1999).
[13] T. Ando, K. Ikeda, and A. Tohsaki, Prog. Theor. Phys. **64**, 1608 (1980).
[14] N. Yamaguchi, T. Kasahara, S. Nagata, and Y. Akaishi, Prog. Theor. Phys. **62**, 1018 (1979); R. Tamagaki, Prog. Theor. Phys. **39**, 91 (1968).
[15] M. Stanoiu *et al*., Eur. Phys. J. A **20**, 95 (2004).
[16] A. Ozawa *et al*., Nucl. Phys. **A691**, 599 (2001), and references therein.
[17] S. Raman *et al*., At. Data Nucl. Data Tabl. **36**, (1987).
[18] N. Itagaki, S. Hirose, T. Otsuka, S. Okabe, and K. Ikeda, Phys. Rev. C **65**, 044302 (2002).
[19] N. Tajima, S. Takahara, and N. Onishi, Nucl. Phys. **A603**, 23 (1996).
[20] Y. Kanada-En'yo and Y. Akaishi, Phys. Rev. C **69**, 034306 (2004).
[21] V. R. Pandharipande, Nucl. Phys. **A738**, 66 (2004).
[22] P. Navrátil, J. P. Vary, and B. R. Barrett, Phys. Rev. C **62**, 054311 (2000).
[23] T. Neff and H. Feldmeier, Nucl. Phys. **A738**, 357 (2004).